Supplementary material for "Frequency- and depth-dependent target strength measurements of individual mesopelagic scatterers" by *Bassett et al.* (2020)

1 PVDF Array

A schematic of the PVDF receiver array is shown in Fig. 1. The Edgetech system samples simultaneously on all eight channels. When using only the inner sectors of the array the structure is similar to that of many four-sector split beam transducers. Based on a theoretical formulation (*Medwin and Clay*, 1998) the full beamwidth at the center frequency of the 30 kHZ BB channel, $f_c = 31.5$ kHz, is 4.6°.

2 30 kHz BB Channel Processing

Signals received by the inner sectors of the PVDF array are used to process signals from the Edgetech/30 kHz BB channel in a method consistent with the techniques applied to the Simrad

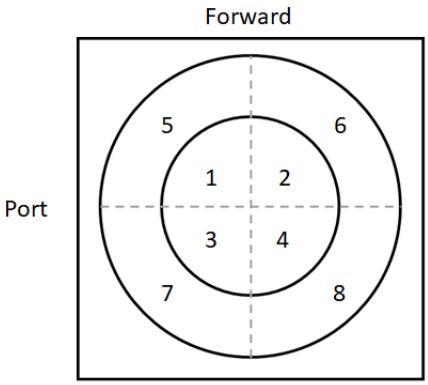

Figure 1: A schematic of the PVDF array. Numbers 1-4 correspond to the inner sectors of the array, which combined have a diameter of 60 cm, are used to process 30 kHz BB data. The other sectors can also be used, thereby resulting in a larger aperture (diameter of 100 cm) with a corresponding narrower beamwidth. The square around the outside of the sectors corresponds to the 110 cm square backing plate.

EK80 (70 kHz BB) channel (*Demer et al.*, 2017). That is, a mean time series, $x(t)$, representing the received signal is calculated from the four inner sectors. Split-beam processing is used to determine the off-axis angle, θ, by calculating the broadband phase relationships between the forward-aft (alongship) and port-starboard (athwartship) combinations. The broadband phase angle, assuming the small angle approximation is valid, is then $\phi = \sqrt{\phi_{al}^2 + \phi_{ath}^2}$, where the subscripts $_{al}$ and $_{ath}$ refer to the along- and athwartship angles. This off-axis angle is then related to the broadband phase by $\theta = \phi/a$, and a is a scalar conversation factor generally referred to as the angle sensitivity. Split-beam processing of this custom system will be included in a future manuscript providing a full working description of the *Deep-See*. The angle sensitivity represents the relationship between the electrical and mechanical angles and is a function of the sound speed and receiver geometry. Off-axis angles can then be used to calculate a theoretical compensation factor, here defined as $\Phi(\theta, f)$ to account for the beam pattern as a function of frequency.

Target strength spectra are calculated according to

$$\mathrm{TS}(f) = 10\log_{10}(|X^2|) + 40\log_{10}(r) + 2\alpha(f)r - 2G(z,f) + \Phi(\theta,f), \tag{1}$$

where X is the Fast Fourier Transform of the selected window from the pulse compressed time series; r is the range to the targets calculated using sound speed profiles and the time delay; α is the attenuation rate in dB/m; and $G(z, f)$ is the frequency- and depth-dependent calibration curve calculated during the on-axis, partial wave calibrations (*Stanton and Chu*, 2008).

To calculate $G(z, f)$ curves, Eq. 1 is re-arranged such that the TS(f) value corresponds to the partial wave response for 20 cm aluminum sphere used in the calibration (*Stanton and Chu*, 2008). The curve is then described by

$$G(z,f) = \frac{1}{2}[10\log_{10}(|X^2|) + 40\log_{10}(r) + 2\alpha r - \mathrm{TS}_{\mathrm{AL20}}(f)]. \tag{2}$$

A comparison between the TS(f) curves calculated for on-axis scattering from the sphere from Eq. 1 or *Demer et al.* (2017), depending on channel, when applying the partial wave calibration curve and the theoretical target strength curve is shown in Fig. 2.

3 Simrad EK80 System and Processing

In post-processing, the 70 kHz transducer was found to have been damaged. Throughout the experiment, including calibration, it was transmitting approximately 50% less power on one of the four sectors. In addition, the received voltage signal times series for the same sector were much lower, resulting in received power time series data approximately 40 dB below the other channels. Despite these differences, real and imaginary components of the received voltages were in-phase across channels. Likewise, the matched-filter envelopes agreed with the exception of the offset in magnitude. The calibration was also performed with these settings (e.g., see Fig. 2).

Since split-beam processing is driven by phase differences between the sectors, the good phase agreement suggests the split-beam processing was not compromised by these problems. A dockside post-calibration was performed to investigate the impact on the beam patterns. An undamaged version of the transducer model has a roughly axi-symmetric 7° beamwidth. The damaged transducer had a slightly modified beampattern with maximum beamwidths of less than 8° in both the along- and athwartship directions. Due to the relatively small differences in the calibration using these parameters, the additional impact of the damaged transducer on 70 kHz BB TS(f) measurement is expected to be less than 1 dB for targets following the quality control criteria.

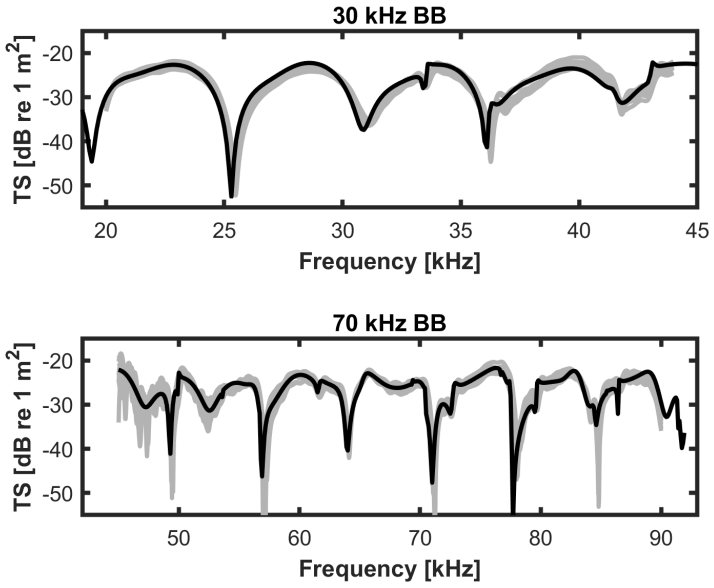

Figure 2: TS spectra from a 20 cm solid AL sphere for the 30 kHz BB and 70 kHz BB channels as determined by applying the partial wave calibration curves. The black lines show the theoretical target strength and gray lines are data from individual pings.

4 General Processing Notes

Targets in both the 30 kHz BB and 70 kHz BB channels were processed using 0.5 m windows. These windows were centered around the peak in the pulse compressed data associated with each target. The use of different window sizes was explored in the initial analysis stages. Window lengths ranging from 0.3 to 1.0 m were explored. Spectral characteristics did not vary with window length, indicating that windows as short as 0.3 m sufficiently captured the relevant portions of the pulse compressed signal from the targets. Therefore, shorter window lengths could have been used. However, due to the relatively high decimation rate a window length of 0.5 m was used so that more data points from the 30 kHz BB channel could be used in the Fast Fourier Transforms. The primary benefit of a 0.5 m window compared to a longer window related to the relative density of animals at some depths. Where higher densities of animals were observed the use of a 1 m window resulted in fewer windows where the response of an individual target could be calculated without including information associated with echoes from different scatterers. As such, the 0.5 m window represents a good balance between capturing the relevant scattering physics and reducing interference between echoes from "adjacent" targets where relative animal densities are high.

The "quality control" processing steps described in the Methods note that different procedures were used for the two channels and that these were driven by the different beamwidths and signal-to-noise ratios. The narrower beamwidth of the PVDF array relative to the 70 kHz BB transducer results in an acoustic footprint that is approximately 50% smaller for the 30 kHz BB channel. Therefore, any target passing through the beam would be expected to be present within the main

lobe for fewer pings. The limits for accepted off-axis targets used in processing were 2.5° and 3.0° for the 30 kHz BB and 70 kHz BB channels, respectively. The ratio of the acoustic footprints is ≈0.7. This value is approximately equal to the ratio of the average pings per target in each channel and shows the beampattern is a key parameter in the number of observed pings per target. Histograms of the number of pings-per-target were consistent as a function of depth, suggesting it played no role in the observed TS(f) and spectral classifications.

Averaging over multiple pings can reduce noise in spectra and produce a more representative curve, assuming that the target has not considerably changed its orientation or shape in a way that meaningfully changes the scattering. Here, the total number of pings per target was limited by the tow-body's speed, any motion of the targets, the range to the targets, and the beamwidths. Larger numbers of pings per target may have meaningfully altered the observed spectra. However, we note that structural similarities are observed between TS(f) curves derived from as many as eight pings and those including fewer pings (down to one in the case of the 30 kHz BB channel). This suggests that any biases introduced by the inclusion of targets with few detections is likely to be small. One reason for this is that in many cases the dominant targets fall into three categories in the 30 kHz BB channel: resonant (R), near-resonance (N), and Rayleigh/below resonance (B). Scatterers classified as R and B are both inherently omnidirectional scatterers and, as a result, additional pings could reduce noise, but would not otherwise be expected to change from ping-to-ping. Scatterers observed near-resonance also exhibit this behavior but to a lesser degree. Scatterers falling into the "flat" and "complex" categories are more complex in this regard. To address this the processing procedures removed individual pings that were in strong disagreement with the others selected for the target. Likewise, targets exhibiting non-physical spectral slopes (e.g., -20 dB over 20 kHz) were assumed to have been further off-axis than indicated by the split-beam processing due to phase wrapping. These targets were also removed.

The best solution to the challenges laid out in this section is to collect greater quantities of data so that larger numbers of targets, ideally with numerous detections meeting quality control criteria, can be used. This was not possible during the early deployments of the *Deep-See* that are presented here.

5 Shipboard EK60 Data

Shipboard echosounder measurements (EK60 18 kHz and 38 kHz) were obtained during the *Deep-See* deployments. These measurements are not co-spatial with the *Deep-See* measurements due to the offset of the tow-body at depth. Nonetheless, if these ship-based measurements are representative of the *Deep-See* observations they can be used to support, or contradict, the observations of the depth profiles of target strength.

Fig. 3 includes echograms from the 18 kHz and 38 kHz channels throughout *Deep-See* deployment, the difference between the channels ($\Delta S_v = S_{v,18kHz} - S_{v,38kHz}$), and depth averaged S_v measurements. *Deep-See* started sampling at 70 m and progressed to deeper depths at intervals of approximately 20 minutes as shown on the echograms. Shallower than 200 m, volume backscattering is higher in the 18 kHz channel. Between 200-400 m the dominant backscattering varies between the two channels with depth and time. From 400-650 m the 38 kHz channel dominates volume backscattering. Below 650 m volume backscattering is similar in both channels with slightly higher backscatter at 18 kHz. Observations of ΔS_v from the shipboard measurements generally agree with TS distributions observed using the 30 kHz BB channel.

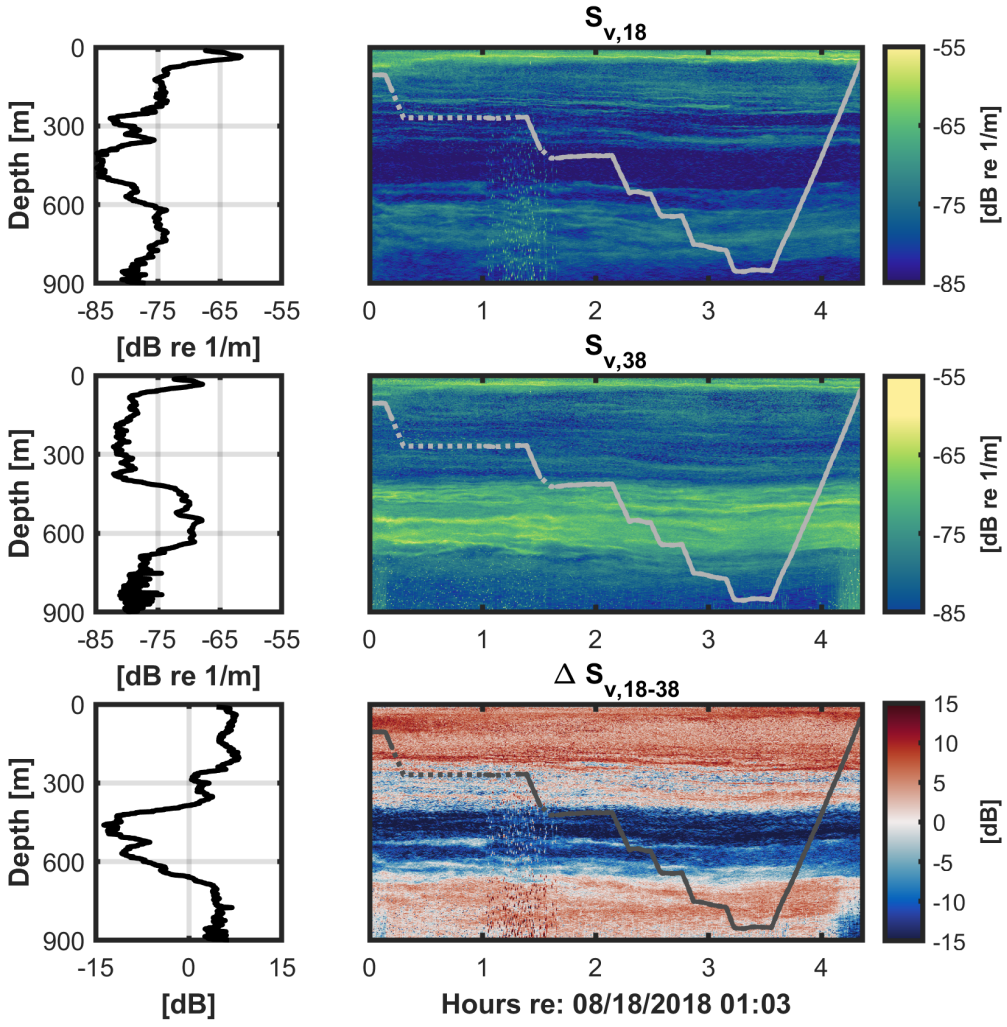

Figure 3: Echograms for the shipboard 18 kHz and 38 kHz channels corresponding to the period for which *Deep-See* data are presented. The left column show the depth averages of the data presented in the echograms. Clear differences in volume backscattering are observed as a function of depth. The dashed portion of the line in the echograms denotes interpolation during a period when the CTD on the *Deep-See* was turned off.

References

Bassett, C., A.C. Lavery, T.K. Stanton, and E. Cotter (2020). "Frequency- and depth-dependent target strength measurements of individual mesopelagic scatterers." *J. Acoust. Soc. Am.*, **148**(2), EL1–EL6.

Medwin, H., and C. S. Clay (1998). *Fundamentals of Acoustics Oceanography* (Academic Press, Boston), pp. 138-141; 290-291.

Stanton, T.K. and D. Chu (2008). "Calibration of broadband active systems using a single standard spherical target." *J. Acoust. Soc. Am.*, **124**, 128–136.

Demer, D.A. and L.N. Andersen and C. Bassett and L. Berger and D. Chu and J. Condiotty *et al.*(2017). "2016 USA–Norway EK80 Workshop Report: Evaluation of a wideband echosounder for fisheries and marine ecosystem science." *ICES Coop. Res. Rep. No. 336.*